Thermal and Electrical Performance Study of Cold-Finger ^{3}He Cryostat in Precision Measurement of Quantum Hall Resistance and Single-Electron Current

Young-Seok Ghee, Wan-Seop Kim, Dong-Hun Chae, Bum-Kyu Kim, Jesse Muhojoki, Myung-Ho Bae, and Nam Kim

***Abstract*— The performance of our newly constructed cold-finger cryostat is investigated for quantum Hall resistance (QHR) and single-electron pump (SEP) devices. The cryostat features a vacuum-sealed sample chamber (SC) attached to a 0.3 K plate inside the inner vacuum can. The SC is designed to accommodate both the SEP and the QHR devices with a shielding partition between them. The measured QHR in the chamber approaches the nominal value for filling factor 2 within 20 parts in 10^9. The white-noise level of the SEP module, as obtained from the Allan deviation data, is 4.5 fA/$\sqrt{\text{Hz}}$. We also investigated the thermometry of the SC either under vacuum or filled with ^{3}He gas. We calculated the thermal conductivity of the different heat conduction channels in the sample holder and found the dominant channel to be through the chip carriers not signal lines.**

***Index Terms*— Cryogenics, current measurement, electrical resistance measurement, measurement uncertainty, quantum dots (QDs), thermal conductivity, thermometers.**

I. Introduction

THE cryostat for the quantum Hall resistance (QHR) standard at the Korea Research Institute of Standard and Science (KRISS) is a single-shot ^{3}He cryostat holding the device in liquid ^{3}He [1]. Consequently, the measurement time is limited by the ^{3}He amount times its evaporation rate. The holding time at a base temperature of 0.3 K is typically ∼10 h, which is long enough for the evaluation of the Hall resistance. For a longer evaluation of physical quantities other than the Hall resistance, we designed and set up a cold-finger-type cryostat (CFC) circulating ^{3}He fluid in continuous mode. Our CFC can remain at a base temperature of 420 mK as long as the liquid-He bath is sustained. With the superconducting magnet in the persistent mode, the CFC can be maintained for three days without filling the transfer of liquid He to the He bath. A particular feature of the CFC is its vacuum-sealed sample chamber (SC) that accommodates both QHR and single-electron pump (SEP) devices. The SC is also equipped with a pair of condensing lines through which exchange gases, such as ^{3}He or ^{4}He gases, can be introduced. Thus, the SC can be operated either in vacuum mode or in heat-exchange gas-filled mode.

The purpose of this SC is to combine an SEP and a quantized Hall resistance array (QHRA) (∼MΩ) to convert current into voltage for direct comparison with a Josephson voltage standard (JVS). Assuming that the SEP current and the QHRA resistance are 100 pA and 1 MΩ, respectively, we obtain a converted Hall voltage of 0.1 mV, which is far too low to be applied in metrology. However, we have fabricated the SC with a hope that the current-to-voltage conversion scheme based on quantum standards can be applied in metrology in the future.

As a preliminary experiment, we performed a precision measurement of the QHR at filling factor 2 ($i = 2$) and the SEP current, respectively, in the vacuum mode. The measured resistance deviates from the nominal resistance of the $i = 2$ plateau by 20 parts in 10^9. The results of the SEP current measurement show that we induced a white-noise level of 4.5 fA/$\sqrt{\text{Hz}}$, which is slightly greater than the level of 3.2 fA/$\sqrt{\text{Hz}}$ recorded using our traditional SEP system (Janis ^{3}He wet system) [2], [3].

We also investigated the thermometry and thermal conductance of the SC in both the vacuum and ^{3}He gas-filled modes. Two sets of temperature sensors—Coulomb blockade thermometer (CBT) and CeO_x sensors—were installed onto the SEP and the QHR module, respectively. We confirmed that the CeO_x temperature was as high as 900 mK at the base temperature in the vacuum mode. However, the ^{3}He gas-filled mode could attain a base temperature lower than 460 mK.

This article is an extension of the proceeding paper [4].

II. Experimental Setup

Our CFC consists of a superinsulation-shielded liquid-He dewar equipped with a 14-T superconducting magnet and

Manuscript received August 30, 2020; revised November 14, 2020; accepted November 17, 2020. Date of publication December 3, 2020; date of current version December 24, 2020. This work was supported by the Korea Research Institute of Standards and Science (Research on Redefinition of SI Base Units) under Grant KRISS-2020-GP2020-0003. The Associate Editor coordinating the review process was Dimitrios Georgakopoulos. *(Corresponding author: Nam Kim.)*

Young-Seok Ghee, Wan-Seop Kim, Dong-Hun Chae, Bum-Kyu Kim, Myung-Ho Bae, and Nam Kim are with the Korea Research Institute of Standards and Science, Daejeon 34113, Republic of Korea (e-mail: namkim@kriss.re.kr).

Jesse Muhojoki is with the Department of Applied Physics, School of Science, Aalto University, 00076 Aalto, Finland.

This article has supplementary downloadable material available at https://doi.org/10.1109/TIM.2020.3041820, provided by the authors.

Digital Object Identifier 10.1109/TIM.2020.3041820

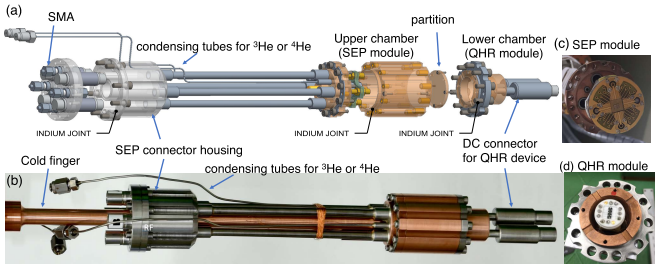

Fig. 1. (a) Drawing and (b) photograph of the SC [4]. (c) Bottom view of the SEP module with a PCB. (d) Top view of the QHR module. The QHR carrier is made of alumina ceramic (white colored part) and is plugged into the receptacle PCB.

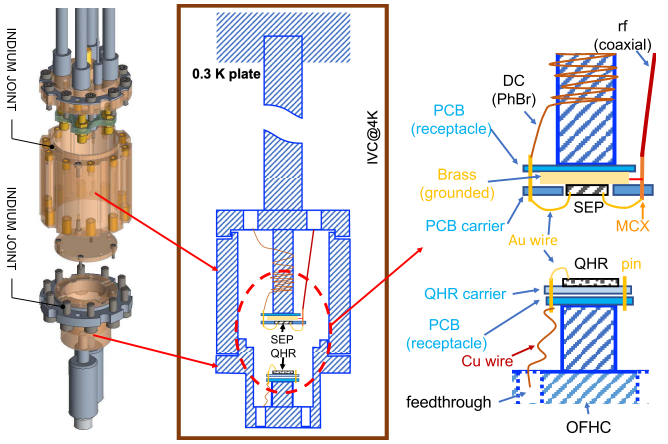

Fig. 2. Drawing of the SC. The wiring configuration and location of the PCBs are shown schematically for the SEP and QHR modules. The partition used to separate the modules was removed because the shielding was not necessary for this experiment.

an insert probe (ICE Oxford Ltd.). The insert probe has a vacuum-sealed SC attached to the 0.3 K plate inside the inner vacuum can (IVC). Fig. 1 shows the SC assembly composed of a cold finger, cryohermetic connectors, and exchange-gas condensing tubes. The cold finger is screwed tight to the 0.3 K plate, whose cooling power is delivered to the device through the cold finger. The SC is partitioned into two separate rooms to accommodate two devices. The role of the partition is to block unwanted electromagnetic interference between the upper and lower chambers. Furthermore, the exchange-gas condensing tubes allow a heat-exchange gas, such as ^{4}He or ^{3}He, into the SC to help cool the device more efficiently. The wiring configuration is intended to minimize the heat conduction to each device for the chosen wires. The details of the wiring configuration are as follows. Six pairs of Cu wires (CDA 101, California Fine Wire Company, AWG 40) for the QHR device are interrupted by superconducting NbTi wires between the 4 K plate and the 1.2 K plate for thermal insulation; by contrast, for the SEP device, 12 pairs of phosphor-bronze (PhBr) wires (Lakeshore, AWG 36) are used. Four coaxial cables are installed for the SEP for their own purposes. A pair of cupronickel coaxial cables (SC-219/50-SCN-CN, Coax. Co) carry radio frequency (RF) signals, and another pair of hybrid coaxial cables (Lemo hybrid cable 280630) are used as source and drain leads. They are also broken by NbTi coaxial cables between the 4 and 1.2 K plates. Flexible coaxial cables (Microcoax HGE055D) are installed inside the SC as replacements for the BeCu semirigid coaxial cables used in the SEP insert of the Janis ^{3}He wet system.

The QHR and SEP devices were placed on chip carriers mated via pins with the corresponding receptacle PCBs [see Figs. 1(c) and (d) and 2]. The receptacle PCBs were all screwed tight onto the oxygen-free high-thermal-conductivity (OFHC) Cu body [see Fig. 4(b)]. The QHR chip carrier is made of alumina, whereas the SEP carrier consists of a G-10 PCB and a brass plate to which the device is attached. Au wires were used for the connections between the devices and the carrier electrodes. Three heat conduction paths exist for the QHR device. One is from the device through the alumina-based carrier via the receptacle PCB (G10) and then to the cold finger (see Fig. 2). The other paths are from Au bonding wires and then either to the receptacle PCB via pin contacts or to Cu wires whose heat is thermally dumped to the OFHC Cu body. A rough estimate indicates that the heat conduction through the first path is dominant over that through the Au-wire paths because of the poor thermal conduction of the wires, which is mainly a consequence of their small cross-sectional area. The thermal conduction is discussed further in Sections III-C and III-D and in the Supplementary Materials. The SEP cooling channels provide roughly four heat conduction paths. For instance, heat flows toward the cold finger from the device through the following four paths in parallel: 1) the brass plate of the SEP chip carrier and the receptacle PCB (G10); 2) the brass plate of the SEP chip carrier, MCX connectors, and coaxial sheaths; 3) the Au bonding wires and PhBr wires; and 4) the Au bonding wires and coaxial cables (see Fig. 2 and the table in the Supplementary Materials for additional details). Our analysis shows that, among these four paths, path 1) is dominant; this path will be discussed again in Sections III-C and III-D and in the Supplementary Materials.

III. Results and Discussion

A. Performance of the QHR Module

The quantized Hall resistance at $i = 2$ in the SC was evaluated using a cryogenic current comparator resistance bridge via a 100-Ω resistance reference, traceable to the KRISS QHR standard [1]. The resistance value deviates from the nominal value for $i = 2$ by 20 parts in 10^9 with an uncertainty of eight parts in 10^{10}, which may arise from an inefficient cooling of QHR device in the cold finger in the vacuum mode. We found that the deviation still persisted even in the ^{3}He-filled mode. We need further study on the origin of the deviation.

Fig. 3(a) shows an Allan deviation of the bridge voltage difference. It follows the inverse-square-root time dependence of white noise (red dotted line) up to the sampling time of 10^3 s. For longer sampling times, the flicker noise regime, as indicated by flattening of the Allan deviation plot (blue dashed line), is started at about 10^3 s. This result is similar to that for the KRISS QHR standard [5].

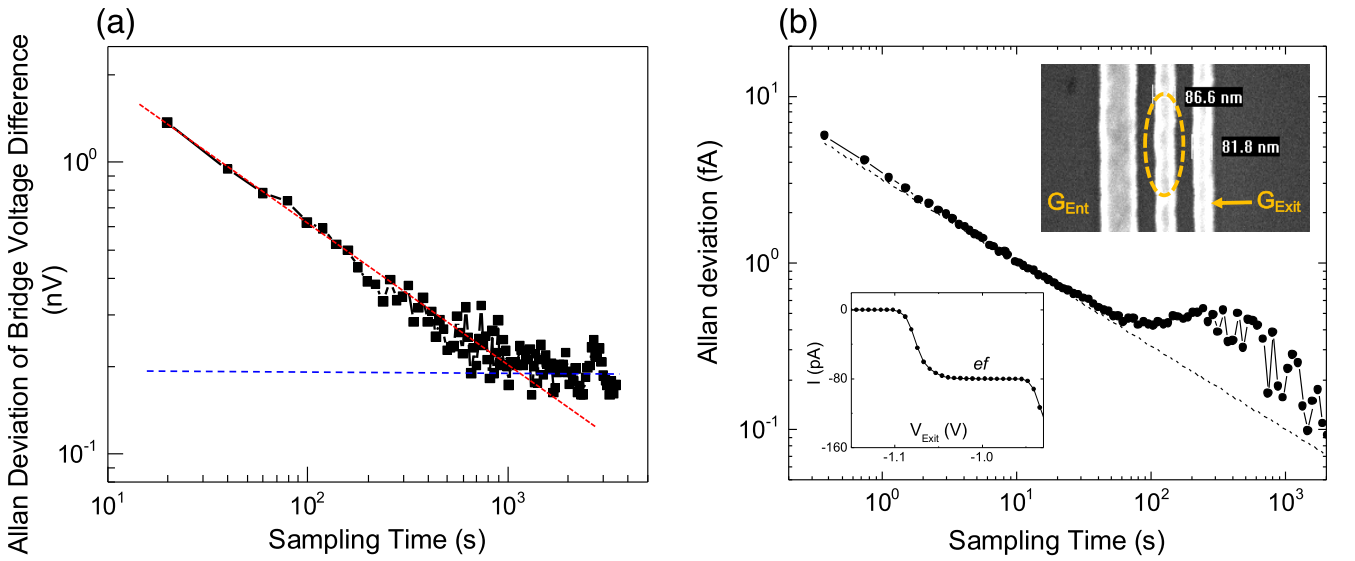

Fig. 3. (a) Allan deviation of the bridge voltage difference for the comparison measurement between the QHR and the 100-Ω resistance reference [4]. (b) Allan deviation obtained from the SEP-current signal with the SEP in a pinched-off state by applying a negative bias to the gates. The SEP current was monitored through the ULCA. The dashed–dotted line represents the relation $\sigma_I = \sqrt{S_I}/\sqrt{\tau}$, where $\sqrt{S_I} = 4.5$ fA/$\sqrt{\text{Hz}}$. The bottom-left inset shows the pumped current curve around the first current plateau at $f = 500$ MHz under $H = -12$ T at $T_{0.3\,\text{K}} = 410$ mK. The top-right inset shows a scanning electron micrograph of the SEP device with three top metal gates (vertical white electrodes) defining a QD. The three top metal gates cross the mesa, which is approximately 700 nm wide.

B. Performance of the SEP Module

After the QHR evaluation was performed, a single-electron pumping experiment was carried out with the SEP module also in the vacuum mode. The device was prepared with a 2-D electron gas system of a GaAs/AlGaAs heterojunction. The quantum dot (QD) was formed by metallic top gates, as shown in the inset of Fig. 3(b). The SEP operation followed our conventional tuning process [6]. We used the low-noise hybrid coaxial lines as the drain lead lines that were connected to the ultrastable low-noise current amplifier (ULCA, Magnicon GmbH) with a nominal transresistance-amplifier gain of 1×10^9 V/A. The SEP was modulated by an RF signal of $f = 500$ MHz to generate ~80 pA corresponding to ef, where e is the elementary charge [see the left inset in Fig. 3(b)]. To investigate the white-noise level $\sqrt{S_I}$ of the system, we measured an Allan deviation at the pinched-off state of the SEP, which was induced by applying V_{Exit} less than -1.1 V. Fig. 3(b) shows the Allan deviation data obtained following our conventional process [2]. The precision measurement of the current plateau was performed with another device that gave a provisional type-A uncertainty of 7×10^{-7} at $I_p \sim 80$ pA (data not shown).

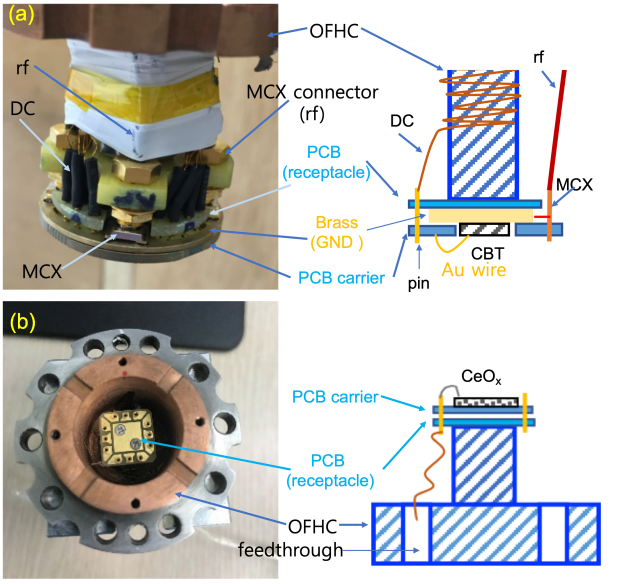

Fig. 4. (Left) Photograph and (right) illustration showing where temperature sensors are installed and how the thermometers are connected to the signal lines in each separate module. (a) CBT on the SEP module and (b) CeO_x sensor on the QHR module.

C. Thermometry

The devices loaded in the SC are not in direct thermal contact with the cold finger anchored to the 0.3 K plate but instead in contact with a poor thermal conducting material such as the G-10 material comprising the PCB. The thermal conductivity of the PCB could be more than 10^5 times worse than that of OFHC Cu. Considering this poor thermal contact for the devices, we needed to measure the device temperature. To estimate the actual device temperature as accurately as possible, we installed two sets of temperature sensors—a CBT and a CeO_x temperature sensor—separately onto the SEP and QHR modules (see Fig. 4). The CBT sensor was installed onto the same carrier as the SEP, whereas the CeO_x sensor was installed onto a G-10-based PCB whose thermal conductivity is known to be lower than that of the alumina-based QHR carrier (for the CeO_x carrier, we could not use the same one as the QHR because the QHR and its carrier is preserved for a QHR standard). According to the literature,

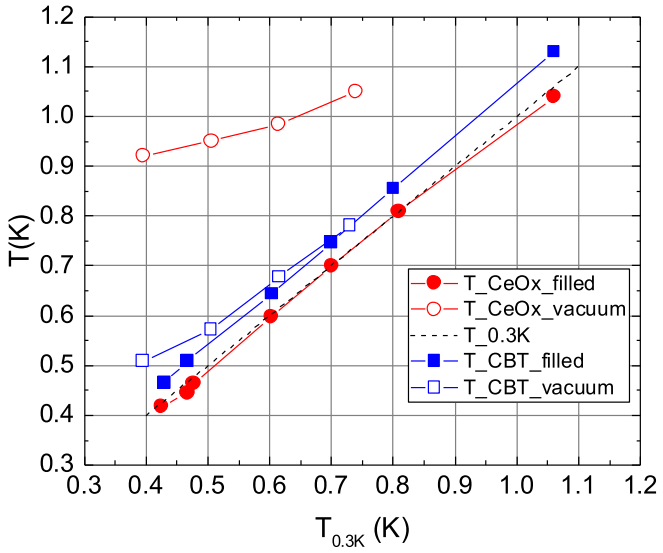

Fig. 5. Thermometry of CBT and CeO_x sensors as a function of the 0.3 K plate temperature, $T_{0.3K}$. Solid squares and circles represent CBT and CeO_x thermometry, respectively, for the ^{3}He gas-filled mode; open squares and circles represent the vacuum mode. The dotted line represents the $T_{0.3\,K}$ value.

the thermal conductivities of alumina and G-10 are 0.1 [7] and 0.02 $Wm^{-1}K^{-1}$ [8] at $T \sim 1$ K, respectively. Thus, the actual thermal conductance of the QHR device could be better than that of the CeO_x sensor at temperatures lower than 1 K.

The CBT sensor is composed of a 10×100 array of Al/AlO_x junctions, whose normal resistance at room temperature is approximately 50 kΩ (see the Supplementary Materials for details). The CeO_x sensor is a commercial one (Lakeshore, CX-1030-SD-HT) that was calibrated in our cryostat with reference to the built-in CeO_x sensor on the 0.3 K plate. During the thermometry, an external magnetic field intensity of 0.3 T was applied to the sensors to suppress the superconductivity of the CBT sensor. This low-intensity magnetic field would not cause a CeO_x sensor error greater than 1%. The CBT sensor, as a primary sensor, is also known to have an error of less than 1% [9].

We investigated thermometry either in vacuum mode or in ^{3}He-filled mode. Vacuum mode means that the SC was maintained under vacuum without any exchange gas; by contrast, in the ^{3}He-filled mode, the SC was filled with ^{3}He gas that would eventually condense into liquid at a base temperature below the transition temperature of ^{3}He gas (∼3.2 K). The amount of ^{3}He transferred to the SC was approximately 6 L in the gas phase, which is believed to condense to a liquid with a volume of 8×10^{-6} m^3, corresponding to the volume of the QHR module.

Fig. 5 shows the thermometry results as a function of the temperature of the 0.3 K plate, $T_{0.3\,K}$. In the ^{3}He-filled mode, the responses of both sensors follow similar trajectories to $T_{0.3\,K}$ line (dotted line) within a difference of approximately 50 mK. However, in the vacuum mode, the T_{CeO_x} data show a different trajectory, increasingly deviating from the dotted line as the temperature decreases. Regarding the CBT sensor, the tendency is similar to that of the CeO_x sensor, but the deviation is much smaller: at most 60 mK at the base temperature. These results imply that, in the vacuum mode, the cooling power for the QHR module could be smaller than that for the SEP module although the different chip carrier was used for the QHR module (see Section III-D for further discussion). We note that the ^{3}He heat-exchange gas provided better cooling for both modules.

The temperature of the CBT sensor, T_{CBT}, was obtained from its differential conductance versus voltage curves via the well-known process [10], [11]. Further details are provided in the Supplementary Materials. At the base temperature, $T_{0.3\,K} \sim 420$ mK, in the vacuum mode, the temperature difference, $T_{CeO_x} - T_{CBT}$, reaches almost 400 mK. We attribute this behavior to the relatively poor thermal conductance between the CeO_x sensor and the OFHC Cu body. In the following discussion, we present our analysis of the thermal conductance of each heat-conducting path.

D. Thermal Conductance Analysis

Fig. 4 shows the zoomed-in photographs and illustrations of the device modules, focusing on how devices are thermally anchored to the cold finger. Both the CBT and the CeO_x sensor are carried on each carrier to be plugged into the receptacle PCBs, which are mechanically coupled by screws to the OFHC Cu body. The OFHC Cu body is assumed to be in thermal equilibrium with the 0.3 K plate. The equilibrium assumption is reasonable because the OFHC Cu body of the module is coupled to the 0.3 K plate via an OFHC Cu rod, the cold finger, as shown in Fig. 1(b), and because the extra heat load imposed by the radiation from the 4 K surface of the IVC and the heat conduction through the remnant gas inside the IVC are estimated to be negligible.

The CBT has three heat conduction paths, in contrast to the four paths for the SEP. The number of paths differs because the fourth heat-conducting path of the SEP, which is through the Au bonding wire, PCB pattern, and coaxial cables, is missing for the CBT. Among these three parallel heat-conducting paths, the path from the brass plate to the PCB is estimated to be the channel with the greatest thermal conductance. A rough estimation indicates that the thermal conductance for the brass-PCB path is 5 mWK^{-1} at 4 K (see the Supplementary Materials for details). Thermal conductance through the dc wires or coaxial cables is estimated to be three orders or one order lower than that of the brass-PCB path, respectively.

On the other hand, the thermal conductance for the CeO_x sensor is estimated to be approximately five times lower than that for the CBT sensor. More specifically, according to our analysis, the dominant thermal conducting paths of the CeO_x sensor are via PCB-to-PCB (see Fig. 4 or Supplementary Material for more detail) and through the sensor lead to the receptacle PCB, whose thermal conductance in summation is estimated to be approximately 1 mWK^{-1}, whereas the thermal conductance through the signal lines of Cu wires is in the order of μW. The poor thermal conductance of the signal lines is mainly due to their small effective cross-sectional area. We note that the estimation of thermal conductance for QHR (not for CeO_x) gives a higher value (∼3 mWK^{-1}) because the

alumina-based carrier was used as the device carrier instead of the G-10-based PCB. As previously mentioned, the thermal conductivity of the alumina material is five times greater than that of the G-10 material at 1 K [7], [8].

Based on our analysis of the thermal conductance, the reason for the temperature discrepancy between the CBT and CeO_x sensors in the vacuum mode of the SC is attributed to the relatively poor thermal conductance of the QHR module. We found that the poor thermal conductance could be improved by using liquid ^{3}He as a heat-exchange cryo-fluid, as shown in Fig. 5. Given that the thermal conductivity of the ^{3}He liquid at 1 K is approximately 0.01 $Wm^{-1}K^{-1}$ [12], which is as low as that of the G-10 material, its ability to help cool the CeO_x sensor to the base temperature is remarkable. We note that T_{CBT} showed the base temperature of 500 mK even in the vacuum mode. This result demonstrates that the brass plate and G-10-based PCB functioned as heat-conducting materials near 500 mK, although the thermal conductance values of these materials at this temperature are not available.

We needed to test ^{4}He gas as another exchange gas to see if the QHR deviation from the nominal value persists or not. However, ^{4}He gas failed to function as an exchange gas because it leaked from the SC presumably when it became superfluid. We suspect that the leak sources were the hermetic feedthroughs such as dc wire connectors and SMA connectors (see Fig. 1, and the model names of the dc and SMA feedthroughs are VB-1B-10 and VB-SMA2, respectively, produced by VACOM Vakuum Komponenten and Messtechnik GmbH), whose interface between the metal pins and their ceramic insulating layer could be a superfluid leak path even though this effect has not yet been proved. We are planning to construct another version of the SC that is superfluid-leak tight.

IV. Conclusion

We investigated the performance of a newly constructed CFC. The CFC was run at base temperature by circulating ^{3}He fluid and features a vacuum-sealed SC that can be operated either in vacuum or ^{3}He gas-filled mode. In the vacuum mode at $T_{0.3\,K} = 410$ mK, precision measurements show that the relative deviation of the measured QHR in the SC from the nominal value is approximately 20 parts in 10^9 and that the Allan deviation of the SEP current gives a 4.5-fA/$\sqrt{\text{Hz}}$ white-noise level. Thus, we speculate that the CFC could be used as a precision measurement system for both SEP and QHR devices, even in the vacuum mode.

By investigating thermometry, we found that the QHR temperature could be much higher than the SEP temperature in the vacuum mode. However, using the ^{3}He gas-filled mode, we could cool devices to lower than 0.5 K.

Acknowledgment

Young-Seok Ghee and Nam Kim are grateful to J. Pekola and A. Manninen for providing the Coulomb blockade thermometer (CBT). Myung-Ho Bae and Bum-Kyu Kim thank Suk-In Park and Jindong Song for their supply of GaAs/AlGaAs heterojunction wafers for the single-electron pump (SEP) investigation.

References

[1] P. Gournay, B. Rolland, D.-H. Chae, and W.-S. Kim, "On-site comparison of quantum Hall effect resistance standards of the KRISS and the BIPM: Ongoing key comparison BIPM EM-K12," *Metrologia*, vol. 57, no. 1, 2020, Art. no. 01010.

[2] M.-H. Bae *et al.*, "Allan-deviation measurements of gate-tunable single electron pumps with the ultrastable low-noise current amplifier," in *Proc. Conf. Precis. Electromagn. Meas. (CPEM)*, Jul. 2018, pp. 1–2.

[3] B.-K. Kim *et al.*, "Precision current measurement with thermal-drift-minimized offset current for single-parameter electron pumps based on gate-switching technique," *AIP Adv.*, vol. 10, no. 4, Apr. 2020, Art. no. 045332.

[4] N. Kim, W.-S. Kim, D.-H. Chae, B.-K. Kim, Y.-S. Ghee, and M.-H. Bae, "Study on cold-finger ^{3}He cryostat for precision measurements of quantum Hall resistance and single-electron pump current," in *Proc. Conf. Precis. Electromagn. Meas. (CPEM)*, Aug. 2020, pp. 1–2.

[5] D.-H. Chae, W.-S. Kim, T. Oe, and N.-H. Kaneko, "Direct comparison of 1 MΩ quantized Hall array resistance and quantum Hall resistance standard," *Metrologia*, vol. 55, no. 5, p. 645, 2018.

[6] M.-H. Bae *et al.*, "Precision measurement of a potential-profile tunable single-electron pump," *Metrologia*, vol. 52, no. 2, pp. 195–200, Apr. 2015.

[7] N. Simon, "Cryogenic properties of inorganic insulation materials for iter magnets: A review," Nat. Inst. Standards Technol., Gaithersburg, MD, USA, Tech. Rep. NISTIR–5030, 1994.

[8] P. Duthil, "Material properties at low temperature," 2015, *arXiv:1501.07100.* [Online]. Available: http://arxiv.org/abs/1501.07100

[9] O. Hahtela *et al.*, "Traceable Coulomb blockade thermometry," *Metrologia*, vol. 54, no. 1, p. 69, 2016.

[10] M. Meschke, J. P. Pekola, F. Gay, R. E. Rapp, and H. Godfrin, "Electron thermalization in metallic islands probed by Coulomb blockade thermometry," *J. Low Temp. Phys.*, vol. 134, no. 5/6, pp. 1119–1143, Jan. 2004.

[11] J. Pekola, K. Hirvi, J. Kauppinen, and M. Paalanen, "Thermometry by arrays of tunnel junctions," *Phys. Rev. Lett.*, vol. 73, no. 21, p. 2903, 1994.

[12] F. Pobell, *Matter Methods at Low Temperatures*, vol. 2. Berlin, Germany: Springer, 2007.

Young-Seok Ghee received the Ph.D. degree in condensed matter physics from Chonnam National University, Gwangju, South Korea, in 2020. During his Ph.D. degree, he studied electronic transport phenomena at low temperature with single-electron pump devices.

He is currently doing post-doctoral research at the Korea Research Institute of Standards and Science, Daejeon, South Korea. He is interested in single-electron transport in 2-D electron gas systems and their applications.

Wan-Seop Kim received the Diploma degree in physics and the Ph.D. degree in experimental condensed matter physics from the University of Duisburg, Duisburg, Germany, in 1993 and 1998, respectively.

From 1999 to 2001, he did research in the field of colossal magnetoresistance in a post-doctoral position at the Korea Research Institute of Standards and Science (KRISS), Daejeon, South Korea. In January 2002, he joined the Center for Electricity, KRISS, where he has been engaged in the development of cryogenic current comparator, quantized Hall resistance measurements, and dc low-current standards. He is in charge of impedance standards.

Dong-Hun Chae received the Ph.D. degree in condensed matter physics from The University of Texas at Austin, Austin, TX, USA, in 2006. During his Ph.D. course, he studied electronic transport phenomena at low temperature through nanoscale devices, including carbon nanotubes and molecules in the single-electron tunneling regime.

His post-doctoral research focused on quantum transport phenomena in the quantum Hall regime and optical properties of layered materials, including graphene and metal dichalcogenides. Since 2006, he had been a Post-Doctoral Research Fellow under the supervision of Klaus von Klitzing at the Max Planck Institute for Solid State Research, Stuttgart, Germany, for five and half years. He joined the Korea Research Institute of Standards and Science, Daejeon, South Korea, in 2012. He is interested in quantum phenomena in solid-state systems and their metrological applications.

Bum-Kyu Kim received the Ph.D. degree in condensed-matter experimental physics from Chonbuk National University, Jeonju, Republic of Korea, in 2014.

In the post-doctoral research period, he focused on quantum transport phenomena in various low-dimensional systems, including carbon nanotube quantum dot and nanohybrid Josephson junctions. In 2018, he joined the Korea Research Institute of Standards and Science, Daejeon, Republic of Korea, where he has been involved in the development of single-electron pump based on GaAs/AlGaAs 2-D electron gas system.

Jesse Muhojoki received the M.Sc. degree in physics from Aalto University, Aalto, Finland, in 2020.

He is specialized in Coulomb blockade thermometry and is interested in metrology in general.

Myung-Ho Bae received the Ph.D. degree in condensed-matter experimental physics from the Pohang University of Science and Technology, Pohang, Republic of Korea, in 2006. He completed five-year post-doctoral research at the Department of Physics and the Department of Electrical and Computer Engineering, University of Illinois at Urbana–Champaign, Champaign, IL, USA, in 2011.

He is currently a Principal Researcher with the Korea Research Institute of Standards and Science, Daejeon, Republic of Korea. His research interests include manipulation of single-electron transport and development of single-electron pumps based on various low-dimensional systems.

Nam Kim received the Ph.D. degree in condensed-matter experimental physics from the Pohang University of Science and Technology, Pohang, Republic of Korea, in 1999.

From 1999 to 2000, he studied mesoscopic transport in carbon-nanotube system in a postdoctoral position at the Korea Research Institute of Standards and Science (KRISS), Daejeon, Republic of Korea. From 2000 to 2002, he did research in the field of metallic single-electron transistor in a post-doctoral position at Jyväskylä University, Jyväskylä, Finland. In 2002, he joined KRISS and is involved in the development of single-electron pump.